High Performance Hybrid-Reluctance-Force-based Tip/tilt System: Design, Control and Evaluation

Ernst Csencsics, Johannes Schlarp and Georg Schitter, *Senior Member, IEEE*

***Abstract*—This paper presents the design, assembly and evaluation of a novel integrated two degree of freedom (2DoF) actuator design for tip/tilt motion and its integration into a fast steering mirror with comparably large range. The system is designed for scanning applications, such as in optical metrology systems, and comprises an integrated symmetric 2DoF hybrid-reluctance-force actuator and mover-flexure-design. The actuator design employs a permanent magnet for biasing the actuator with a constant flux and two actuator coils per axis to generate a steering flux for positioning the mover. The system prototype has an angular range of $\pm 3^\circ$ in tip and tilt and achieves a closed-loop control bandwidth of 1 kHz based on the signal of eddy current sensors. Compared to the only so far realized state-of-the-art reluctance force actuated FSM system with integrated sensors, the presented design enables to improve the product of range times bandwidth, representing a measure for the system performance, by more than 85%.**

***Index Terms*—Reluctance actuator, Flux steering, Tip/tilt system, Flexure design, Fast steering mirror**

I. Introduction

Opto-mechatronic tip/tilt systems, such as fast steering mirrors (FSMs), are employed for a large variety of applications that can be subdivided into pointing and scanning operations. Typical pointing applications include acquisition of optical signals and tracking of objects [1], as well as pointing of laser or light beams [2] and stabilization of optical systems such as in optical free space communication [3]. Scanning applications are even wider spread, ranging from laser scanners [4] over material processing [5] to scanning optical lithography [6] and confocal microscopy [7]. Most common actuation technologies for FSMs are voice coil [4] and piezo actuators [8]. Voice coil actuators are used to design low stiffness systems with larger scan range but limited bandwidth, such as ± 87 mrad and 350 Hz [2], while piezos are used for high stiffness systems with higher bandwidth but limited range, such as ± 2 mrad and 3 kHz [3]. So there is a clear performance tradeoff required when designing such systems as large range and large bandwidth can not be achieved at the same time.

Reluctance force actuators have the potential to lift this tradeoff to a higher level, due to a higher motor constant as compared to voice coil actuators [9] and larger working ranges as compared to piezos. However, due to several challenges such as non-linear force-current and force-gap relations, the high force variation and the ability to exert unidirectional forces only, reluctance actuators have hardly been implemented in high precision positioning and scanning systems in the past [9], [10].

Nevertheless, several reluctance actuation based designs and applications have been reported. Electromagnetic reluctance actuators, linearized by using permanent magnets, with short strokes around 100 μm are designed for linear motion of fast tool servos [11], [12] and are also employed as valve engines [13]. A large high force linear hybrid actuator with a range of ± 1 mm and low stiffness has been developed for the active vibration isolation in precision machines [14], where the term hybrid refers to the use of two different sources of magnetic flux (coils and permanent magnets).

Recently, reluctance actuation has been employed for rotational motion in a FSM system [15]. A FSM with an angular range of ± 3.5 mrad is reported to achieve a closed loop system bandwidth of 2 kHz with internal sensors and 10 kHz with a fast external optical sensor system. The system uses four actuators, with distinct magnetic circuits and biasing magnets, placed around the mover, which enable high accelerations, but limit the incidence angle of an incoming beam and make the system structure rather bulky. More compact concept design studies of this FSM system with comparable angular range have also been developed [16], [17]. However, both concept designs stick to the structure with four distinct actuators and have not been realized so far. With the limited range of the reported systems the question remains, if the benefits of hybrid reluctance actuators can also be employed for FSMs with larger angular range.

This paper proposes a novel hybrid reluctance actuator design for a FSM system with a comparably large angular range of $\pm 3^\circ$ (± 52.4 mrad). The main contributions of this work include (a) the integrated design of the hybrid reluctance tip/tilt actuator, which requires only a single biasing magnet and can be entirely placed behind the mirror/mover plane, (b) the application of a reluctance force actuator for a large range FSM system, (c) the analysis of the combined magnetic circuit and the mechanical system design, and (d) an experimental demonstration of the working principle and the system performance, providing large angular range and bandwidth at the same time. The integrated design of the actuation system with a single permanent magnet and ferromagnetic core is thereby targeted to serve as enabler for very compact FSM designs. After a review of tip/tilt system specifications reported in literature and considering requirements of target applications from the field of optical metrology systems, the performance goals in Table I for the hybrid actuator prototype system were formulated. For enabling mirror apertures of up to 2" the

The authors are with the Christian Doppler Laboratory for Precision Engineering for Automated In-Line Metrology at the Automation and Control Institute, Technische Universität Wien, A-1040 Vienna, Austria. Corresponding author email: csencsics@acin.tuwien.ac.at.

Post-print version of the article: E. Csencsics, J. Schlarp and G. Schitter, "High Performance Hybrid-Reluctance-Force-based Tip/tilt System: Design, Control and Evaluation," *IEEE Transactions on Mechatronics*, vol. 23, no. 5, pp. 2494-2502, 2018. DOI: 10.1109/TMECH.2018.2866272

mover of the prototype system has a diameter of 56 mm.

TABLE I
HYBRID ACTUATOR TARGETED PERFORMANCE GOALS.

Parameter	Performance goal
Angular range	$\pm 3°$ (± 52 mrad)
Bandwidth (-3 dB)	1 kHz
Angular acceleration	5e3 rad/s^2
Angular resolution	5 μrad
Mover diameter	56 mm

Section II-A provides an overview of the system architecture. In Section II-B the working principle of the actuator is discussed and an analysis of the magnetic circuit is presented. The mechanical design, including the flexure, is described in Section III. In Section IV the experimental system is presented and the system dynamics are identified. Section IV-C discusses the controller design and implementation and Section V presents an evaluation of the experimental system results. Section VI concludes the paper.

II. Actuator Description

A. Hardware Overview

The proposed system design relies on two main components. First, an advanced compact two degree of freedom (2DoF) actuator for tip/tilt motion is designed, which is based on a linear motion hybrid reluctance actuator design [18]. The actuator relies on the magnification and attenuation of a magnetic biasing field, which linearizes the actuator with respect to the current, and has a higher force to current ratio than voice coil actuators, thus providing higher accelerations [9], [11]. The actuation concept allows to keep the inertia of the mover minimal with respect to structural considerations, contrary to voice coil actuated systems, that usually suffer from an increased inertia due to the magnetic circuits of the actuator mounted to the outer parts of the mover.

Second, a suspension system comprising a 2DoF flexure mechanism and a pivot bearing is designed to suspend the mover. The suspension system restricts the four non-actuated DoF and is designed to compensate the negative stiffness of the actuator, resulting in a low but positive stiffness of the two actuated DoF (rotation around x- and y-axis).

Fig.1 shows a cross-section view of the actuator along one actuation axis and provides an overview of the main components. The actuator parts with yoke, magnet, coils and mover are observable as well as the restoring flexure, which constrains three of the non-actuated DoFs. The pivot bearing in the center fixes the point of rotation and constraints the fourth non-actuated DoF. The yoke parts of the two system axes are connected below the permanent magnet, so that a single permanent magnet can be used to bias both system axes. For system evaluation eddy current sensors are mounted on the front side of the mover and are used for measuring the position of the mover relative to the housing. In future system designs the sensor system can be integrated below the mover.

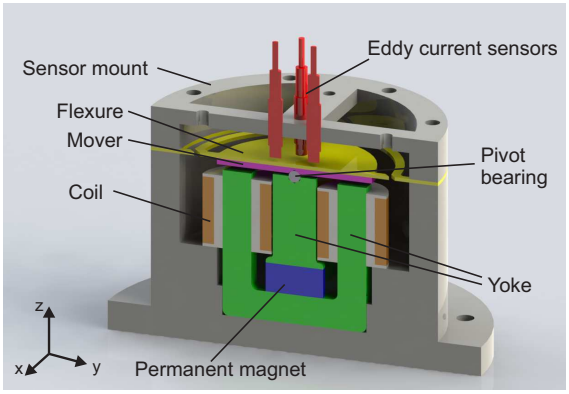

Fig. 1. Cross section view of the hybrid actuator along one system axis. The yoke parts (green), the biasing permanent magnet (blue), the coils (orange), the mover (magenta) and the restoring flexure (yellow) are shown. For evaluation the position of the mover is measured by an eddy current sensor system (red).

B. Hybrid-Reluctance-Force Actuation Principle

The 2DoF hybrid actuator consists of two perpendicularly arranged hybrid-reluctance-force actuators that are combined to one magnetic circuit. The working principle of a single actuator axis is depicted in Fig. 2. In the center of the actuator there is a permanent magnet (blue), which generates a DC biasing flux that passes through the center ferromagnetic yoke part (green), the nonworking air gap, and the ferromagnetic mover (magenta) and returns via the working air gaps and the left and right ferromagnetic yoke part (green), respectively. The DC biasing flux is indicated by the blue lines. When the mover is in the middle position the biasing flux is distributed equally over the left and right air gap, so that there is no net torque on the mover for the case of zero current.

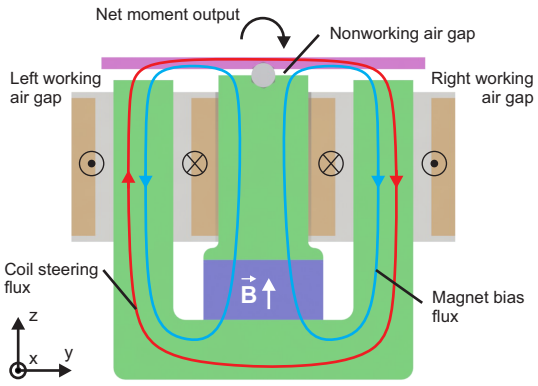

Fig. 2. Schematic of the hybrid-reluctance-force actuation principle. The magnetic circuit is biased by a permanent magnet. The flux due to a coil current strengthens and weakens the flux in the right and left air gap, respectively, resulting in a clockwise torque.

The actuator coils are connected in series so that an applied current generates a magnetic flux (red line) that passes through the outer yoke parts, the mover and the working air gaps in either clockwise (see Fig. 2) or counter-clockwise direction,

Post-print version of the article: E. Csencsics, J. Schlarp and G. Schitter, "High Performance Hybrid-Reluctance-Force-based Tip/tilt System: Design, Control and Evaluation," *IEEE Transactions on Mechatronics*, vol. 23, no. 5, pp. 2494-2502, 2018. DOI: 10.1109/TMECH.2018.2866272

depending on the current direction. As the permanent magnet represents a high reluctance to outer magnetic fields, the coil flux does not pass through the center yoke part. The DC biasing flux and the steering coil flux are superimposed in the two working air gaps. This results in an increased overall flux in the right air gap, as both fluxes are pointing in the same direction, and a reduced flux in the left air gap, yielding a clockwise net torque on the mover. Reversing the current direction will reverse the coil flux and result in a counter-clockwise torque on the mover.

When there is no coil current present, the distribution of the (biasing) flux over the working air gaps is determined by the mover position and the resulting reluctances only. More flux will pass through the shorter air gap resulting in an increasingly high torque on the mover in the direction of the initial displacement. This is equal to a negative stiffness of the actuator and shows that the actuation principle itself is inherently open-loop unstable, due to the insertion of the permanent magnet. Without the permanent magnet, however, the coils would also need to produce the magnetic DC biasing flux, which is a determining factor for the motor constant (see next section) and linearizes the actuator force with respect to the current. This would clearly increase the current consumption and degrade the energy efficiency of the system [18].

C. Analysis of Magnetic Circuit

For showing a more analytic description of the working principle a mathematical analysis of the actuator's magnetic circuit is done. From the 3-dimensional structure and flux paths of the actuator the magnetic circuit model in Fig. 3 can be derived for single axis operation. For simplicity zero

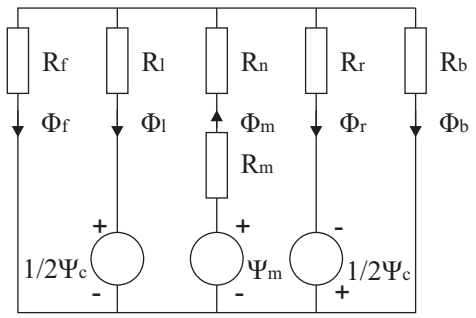

Fig. 3. Magnetic circuit of the 2DoF actuator for single axis operation. The reluctances of and the fluxes through the air gaps are denoted by R_i and Φ_i, respectively. The permanent magnet and the coils are modelled as magnetomotive forces Ψ_m and Ψ_c.

leakage fluxes and infinite permeability of the yoke parts is assumed in the analysis. The two coils are modelled by magnetomotive forces (MMF) $\Psi_c = 1/2Ni_c$, with N the number of coil turns for the entire axis (both coils) and i_c the coil current. The permanent magnet is also modelled as MMF $\Psi_m = H_c l_m$, where H_c is the collectivity and l_m the length of the magnet, with an internal reluctance R_m. The reluctances of the left, right, front, back and nonworking air gap are denoted by R_l, R_r, R_f, R_b and R_n, respectively, and can be calculated by $R_x = l_x/(\mu_0 A_p)$, with μ_0 the permeability of vacuum, l_x the length and A_p the cross section of the air gap. The related fluxes through these air gaps are denoted by Φ with the related indices.

With the derived magnetic circuit the network equations

$$1/2\Psi_c + \Psi_m = (R_m + R_n)\Phi_m + R_r\Phi_r, \quad (1)$$
$$-1/2\Psi_c + \Psi_m = (R_m + R_n)\Phi_m + R_l\Phi_l, \quad (2)$$
$$\Psi_m = (R_m + R_n)\Phi_m + R_b\Phi_b, \quad (3)$$
$$\Psi_m = (R_m + R_n)\Phi_m + R_f\Phi_f, \quad (4)$$
$$0 = \Phi_m - \Phi_r - \Phi_l - \Phi_b - \Phi_f \quad (5)$$

can be obtained. Solving the network equations for the unknown magnetic fluxes and using the derived fluxes in the left and right air gap, the resulting torque generated by the actuator can be calculated by

$$T_A = \frac{\Phi_r^2 - \Phi_l^2}{2\mu_0 A_p} \cdot r_F, \quad (6)$$

with r_F being the lever arm.

A key result of this analysis is that the actuator torque output is linear with respect to the coil current, which is a direct result of the biasing flux of the permanent magnet. This can be shown by simplifying the results of the analysis for the middle position of the mover. With $R_{mag} = R_m + R_n$ and under the assumption that $R_{mag} >> R_{l,r,b,f}$ the flux in the the right and left air gap when the mover is in the middle position ($R_l = R_r = R_b = R_f = R$) can be approximated by

$$\Phi_r\Big|_{midPos} \approx \frac{\Psi_c}{2R} + \frac{\Psi_m}{4R_{mag}}, \quad (7)$$
$$\Phi_l\Big|_{midPos} \approx \frac{-\Psi_c}{2R} + \frac{\Psi_m}{4R_{mag}}. \quad (8)$$

With the approximated fluxes from (7) and (8) and by substituting the expressions for the reluctances and MMFs the actuator torque in the middle position is

$$T_A\Big|_{midPos} \approx Ni_c \cdot H_c \frac{l_m}{l_m + l_n} \cdot \frac{\mu_0 A_p}{4l_{w0}} \cdot r_F, \quad (9)$$

with l_{w0} being the length of the working air gaps in the middle position. This result also shows that the magnet properties and dimensions are significantly influencing the force to current ratio of the actuator. However, a position dependency of the force to current ratio still remains due to an increased biasing flux at mover positions close to the yoke parts, resulting in a higher force to current ratio at larger angular deflection. To check the validity of the derived relations the torques resulting from the analytic calculation are compared to results of a FEM simulation. In Fig. 4a this comparison is depicted for currents of 2 and 4 A. For deflection angles smaller than $\pm 2°$ the analytic results show good agreement with the simulation results, while at larger displacements there is a notable divergence between analytic calculation and simulation, which may be due to stray flux. At large negative angular displacements a current of 6 A generates less torque than lower currents. This is because the generated coil steering flux already exceeds the magnet bias flux, such that the resulting flux density vector changes its direction in the air gap where magnet bias and

Post-print version of the article: E. Csencsics, J. Schlarp and G. Schitter, "High Performance Hybrid-Reluctance-Force-based Tip/tilt System: Design, Control and Evaluation," *IEEE Transactions on Mechatronics*, vol. 23, no. 5, pp. 2494-2502, 2018. DOI: 10.1109/TMECH.2018.2866272

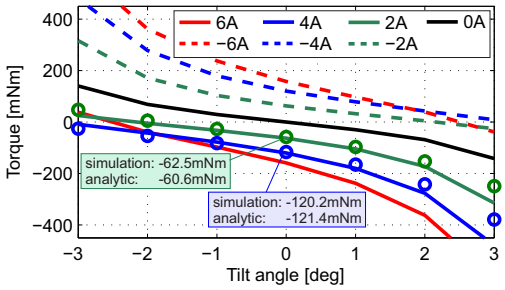

(a) Without flexure

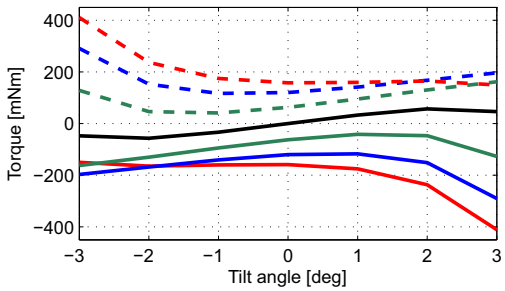

(b) With flexure

Fig. 4. FEM simulated torque curves (force lever 20 mm) of the hybrid actuator at varying coil currents. (a) shows the torque of the actuator only, clearly illustrating its negative stiffness. The torque values resulting from the analytic calculation are marked by 'o' for currents of 2 and 4 A. (b) depicts the torques when the mover is attached to a restoring flexure with positive stiffness.

coil steering flux have opposing directions. This reduces the difference of the squared fluxes in (6), leading to a reduced torque.

The reactance of the inductive actuator load is increasing with frequency, such that the maximum terminal voltage at the driving amplifier output will limit the maximum output current at higher frequencies. Considering this fact and using the analysis given above in a parametric study, yields the final actuator design with 70 turns per coil and a permanent magnet (NdFeB) with a diameter of 20 mm, a height of 10 mm and a flux density of 1.25 T.

Considering the target bandwidth of the system, additional dynamics introduced by eddy currents in the ferromagnetic yoke parts, particularly a phase lag that limits the achievable closed-loop bandwidth, were investigated, simulated and modelled [19]. Analysis showed that a solid configuration of the outer yoke parts (10x10 mm cross section) would cause a phase lag that limits the bandwidth to below 400 Hz. The outer yoke parts, denoting the high frequency flux paths, are thus made of isolated 0.5 mm steel sheets (EN 10025 S 235 JR) to reduce eddy current effects. As the center yoke part is passed by the biasing DC flux only, this part is made out of a solid material.

III. Mechanical System Design

The mechanical system design is crucial for achieving a high system performance. It needs to provide sufficient structural stiffness and a suitable suspension structure. From an integrated system design's perspective, also considering the system complexity, the following design goals are proposed:

- Decouple the two actuated DoFs of the mover to enable an efficient architecture and precise control.
- Provide low stiffness in the actuated DoF to enable large angular range and restrict all other DoF.
- Place structural modes of the flexure and the mover well above the crossover frequency in order to increase the stability margins of the system.

The first goal is met by a perpendicular arrangement of the actuator axes and a suitable flexure design that allows rotations (low stiffness) around x- and y-axis while constraining translational motions along these axes and rotational motions around the z-axis (high stiffness). The flexure is designed to slightly over-compensate the negative stiffness of the actuator in order to stabilize the inherently unstable actuation principle (see Section II-B), resulting in an open loop stable system. Fig. 4a, shows FEM simulation results of the pure actuator torque for different coil currents, clearly illustrating the system's inherent negative stiffness. In Fig. 4b the actuator torque is superimposed with the restoring torque of the designed flexure, which results in an overall slightly positive system stiffness and a reduced position-dependency of the motor constant over a wide actuation range, reducing the variation to 30-72 mNm/A over the entire range. The flexure design can thus also be employed for achieving the second design goal.

The ferromagnetic mover, with a diameter of 56 mm and a thickness of 3.5 mm, is bonded to the flexure as shown in Fig. 5a. Due to the biasing flux of the permanent magnet a high offset force occurs in z-direction (28 N at 0 A, 37 N at 6 A). To avoid damage of the flexure an additional pivot bearing is used (see Fig. 1) to react the z-forces and to fix the point of rotation. The entire actuator is placed in a solid aluminium base that provides sufficient structural stiffness and has an outer diameter of 100 mm. A modal analysis of the flexure with *ANSYS* (Ansys Inc., PA, USA) reveals a suspension mode at 103 Hz and a first structural mode at 1.39 kHz which is already well above the targeted crossover frequency. The first two mode shapes of the flexure are depicted in Fig. 5b and 5c. The first structural mode of the entire mover occurs above 10 kHz. The resulting prototype system has an outer diameter of 100 mm and a height of 70 mm.

IV. Realization of Actuator Prototype

A. Setup Components

A block diagram of the realized experimental prototype system setup is depicted in Fig. 6c. Each actuator axis ($G_{xx}(s)$ and $G_{yy}(s)$) is driven by a custom made current amplifier $A(s)$ (Amplifier type MP38CL, Apex Microtechnology, Tucson, AZ, USA). Due to the actuator inductance of about 1 mH (140 coil turns per axis) the power amplifiers need to provide high current and voltage at higher drive frequencies. The actuator resistance of 5.3 Ω further represents a small ohmic load, such that the amplifiers also have to internally dissipate the majority of the required power. To stay within the thermal limits of the amplifiers the supply voltage is set to 30 V and an appropriate heat sink is attached. The amplifiers are

Post-print version of the article: E. Csencsics, J. Schlarp and G. Schitter, "High Performance Hybrid-Reluctance-Force-based Tip/tilt System: Design, Control and Evaluation," *IEEE Transactions on Mechatronics*, vol. 23, no. 5, pp. 2494-2502, 2018. DOI: 10.1109/TMECH.2018.2866272

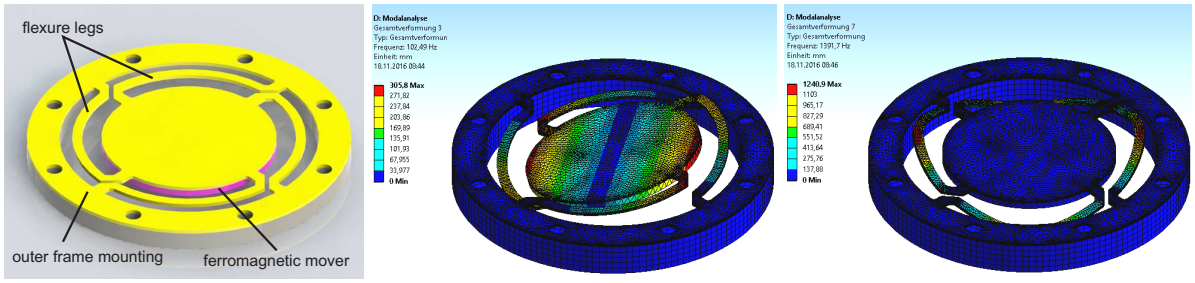

(a) CAD rendering (b) Suspension mode (c) 1st structural mode

Fig. 5. Designed aluminium flexure for restoring mover position. (a) shows a CAD rendering of the designed flexure (yellow) with the bonded mover (magenta). (b) and (c) depict the results of the modal analysis, showing the suspension mode (102.5 Hz) and the first structural mode (1.39 kHz), respectively.

controlled by PI current controllers $C_A(s)$ with a bandwidth of 30 kHz, implemented on the FPGA of a dSpace-platform (Type: DS1202, dSPACE GmbH, Germany). For measuring the rotational position of the mover in 2DoF one differential eddy current sensor system $E(s)$ (eddyNCDT DT3702-U1-A-C3, Micro-Epsilon GmbH, Germany) is used per system axis, as depicted in Fig. 6a. In Fig. 6b the open system with the layered outer yoke parts, two actuator coils, the solid center yoke part and the pivot bearing is shown. For identification of the system dynamics a system analyzer (3562A, Hewlett-Packard, CA, USA) is employed. To identify the system dynamics for the design of position controllers, the reference inputs $I_{x,ref}$ and $I_{y,ref}$ of the current control loops and the signals Θ_x and Θ_y of the position sensors are considered as the system inputs and outputs, respectively.

B. System Identification

The frequency response data of both system axes is shown in Fig. 7. The suspension mode of the x- and y-axis lies at 109 Hz and 107 Hz, respectively, which are in good agreement with the FEM simulations. The zero-pole-pair at 1.35 kHz is the first structural mode of the designed flexure (predicted by simulations) and is similar for both axes. The structural mode is well above the targeted crossover frequency of about 500 Hz and is not a limiting aspect from controls perspective. The stiffness of the system changes with the amplitude of the drive current, as the negative stiffness of the actuator increases at larger displacements, reducing the resulting overall stiffness of the system. This can be seen from the zoomed low frequency range insert in Fig. 7, which shows the spring line of the system at different drive currents. The slope is shifted from -11 dB (at 500 mA) to -8 dB (at 2 A). It is not possible to operate the system at current amplitudes larger than 2 A without position feedback, as the mover snaps to the ferromagnetic yoke parts at larger displacements. Accordingly also the resonance frequency of the system shifts to lower frequencies for larger current amplitudes. The mass line, however, remains unchanged for varying drive currents, as the inertia of the mover is constant. As the system is to be controlled with bandwidths larger than the suspension mode [20], the non-linearity at low frequencies is not a critical factor.

The system shows an increasing phase lag with higher frequencies, which is mainly the result of eddy current losses in the high frequency flux paths [19] and to a lower extend due to the sensor dynamics. The noise floor of the system is reached at about 65 dB.

The dynamics of the system axes can both be modelled by the same fourth order transfer function(TF)

$$P(s) = K \cdot \frac{\omega_0^2}{s^2 + 2\omega_0\zeta_0 s + \omega_0^2} \cdot \frac{s^2 + 2\omega_1\zeta_1 s + \omega_1^2}{s^2 + 2\omega_2\zeta_2 s + \omega_2^2} \cdot e^{sT_d}, \quad (10)$$

with K=1.298e5 and parameters according to Table II. A time delay of T_d = 100 μs is used to model the phase lag of the system.

For investigation of the mechanical crosstalk between the actuator axes, illustrated by the blocks $G_{xy}(s)$ and $G_{yx}(s)$ in Fig. 6c, the magnitude response of the crosstalk TFs are measured (data not shown). The magnitude of the crosstalk at DC is more than 21 dB smaller than the magnitude of the axis TFs. At the suspension mode the attenuation still amounts to -12 dB. This justifies the application of one SISO controller per axis, which is designed in the next section.

TABLE II
COEFFICIENTS OF THE ACTUATOR SYSTEM MODEL.

Index	ω_{Index} [rad/s]	ζ_{Index}
0	679	0.031
1	8.23e3	0.003
2	8.36e3	0.004

C. Controller design and implementation

The design of the position controllers $C_P(s)$ for both system axes is done with the aim of maximizing the crossover frequency, while maintaining a phase margin of at least 30°. Based on the identification data a PID controller is designed for a crossover frequency of 500 Hz according to the tuning rule in [21]. The P-gain is used to shift the intersection of mass- and 0 dB-line to the targeted crossover frequency, while the D-gain is designed to maximize the phase lead at crossover. The differential action is stopped by a realization term that generates a pole at 1.65 kHz to limit the control effort at

Post-print version of the article: E. Csencsics, J. Schlarp and G. Schitter, "High Performance Hybrid-Reluctance-Force-based Tip/tilt System: Design, Control and Evaluation," *IEEE Transactions on Mechatronics*, vol. 23, no. 5, pp. 2494-2502, 2018. DOI: 10.1109/TMECH.2018.2866272

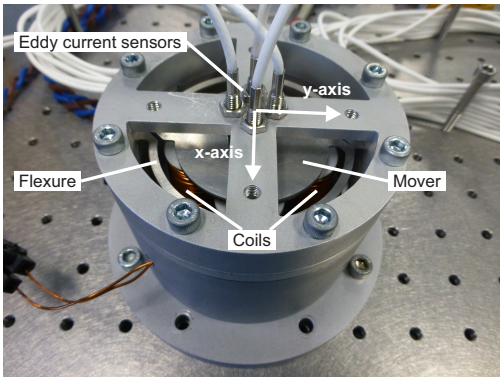

(a) Actuator with sensor system

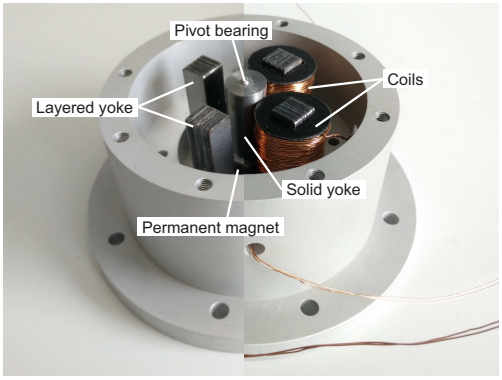

(b) Open actuator

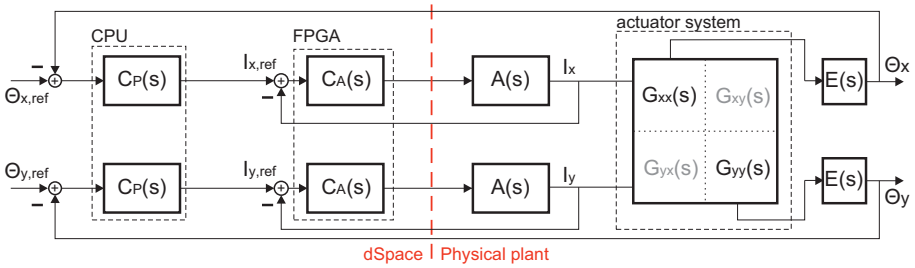

(c) Block diagram of experimental system setup

Fig. 6. Experimental hybrid actuator setup with eddy current sensors. (a) shows the closed setup with the sensors mounted on top of the mover. (b) depicts the open actuator, showing the layered yoke parts with the coils, the solid center yoke part and the permanent magnet. (c) shows a block diagram of the experimental setup system structure.

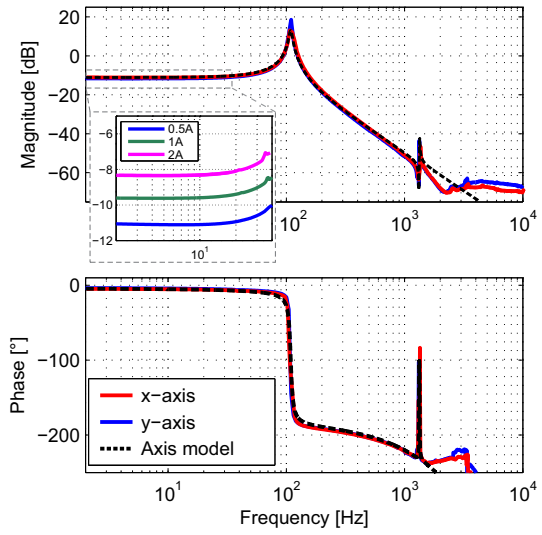

Fig. 7. Frequency response of actuator x- (solid red) and y-axis (solid blue) and the system axis model (dashed black) at 500 mA. The input is the drive current, the output is the position sensor signal. The zoomed images show the low frequency range with increased drive currents, illustrating the operation dependent stiffness of the actuator.

higher frequencies. The I-gain is used to increase the loop gain at low frequencies in order to reduce the steady state error of the system [18]. To attenuate the resonance of the flexure's structural mode an additional notch filter is applied at 1330 Hz. This results in a controller of the form

$$C_P(s) = K_C \cdot \frac{\left(\prod_{i=1}^{2} s^2 + 2\zeta_{z_i}\omega_{z_i}s + \omega_{z_i}^2\right)}{\left(s^2 + 2\zeta_{p_1}\omega_{p_1}s + \omega_{p_1}^2\right) \cdot \left(\prod_{i=2}^{3} s + \omega_{p_i}\right)}, \quad (11)$$

with gain K_C=224 and coefficients according to Table III. As the TFs of both system axes are similar the same controller can be applied to both axes.

TABLE III
COEFFICIENTS OF THE PID CONTROLLER.

Index	ω_{Index} [rad/s]	ζ_{Index}
z_1	552	0.893
z_2	8.38e3	0.006
p_1	8.38e3	0.03
p_2	6.28	-
p_3	1.04e4	-

For implementation in the processor of the dSpace system the controllers are discretized for a sampling frequency of f_s=45 kHz by using Pole-Zero-Matching [22]. Using the

Post-print version of the article: E. Csencsics, J. Schlarp and G. Schitter, "High Performance Hybrid-Reluctance-Force-based Tip/tilt System: Design, Control and Evaluation," *IEEE Transactions on Mechatronics*, vol. 23, no. 5, pp. 2494-2502, 2018. DOI: 10.1109/TMECH.2018.2866272

relation $z = e^{s/f_s}$, poles and zeros are directly transformed to the discrete time domain, ensuring that the notch filter is located exactly at the dedicated frequency.

V. Evaluation of System Performance

The performance of the tip/tilt system is evaluated in terms of achieved bandwidth, angular range, angular resolution and current consumption. Further also the area of operation of the system, which characterizes feasible frequency/amplitude combinations of the reference signal, and the dual axis operation is evaluated.

The measured open loop frequency response (magenta) of one actuator axis with the implemented controller is shown in Fig. 8. The system shows a crossover frequency of 470 Hz, has a phase margin of 31° and a gain margin of 4.7 dB. As intended, the notch filter compensates the structural mode of the aluminium flexure. The complementary sensitivity function (black) of the system is also shown in Fig. 8. It shows a -3 dB bandwidth of 1 kHz and a maximum peaking of 6 dB at 550Hz. The zero of the structural mode causes the magnitude drop just above the system bandwidth.

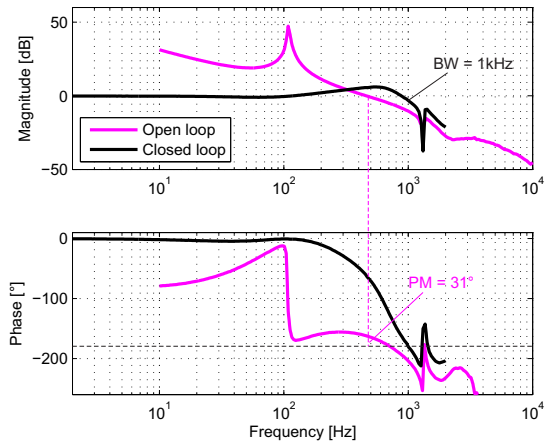

Fig. 8. Open loop (magenta) and complementary sensitivity function (black) of one actuator axis. The open loop plot shows a phase margin (PM) of 31° at a crossover frequency of 450 Hz. The closed loop plot shows a 3 dB system bandwidth of 1 kHz.

To measure the area of operation of the closed-loop system, describing feasible frequency/amplitude combinations, a sinusoidal reference signal is applied to one system axis. The frequency of the reference signal is varied from 1 Hz to 1 kHz and the amplitude at each frequency point is maximized until either the current limit or the maximum terminal voltage is reached. The resulting area of operation with the implemented controller is depicted in Fig. 9a, with the green area illustrating feasible frequency/amplitude combinations. It can be seen that for a sinusoidal reference the system can be operated with the maximum scan range of ±52.4 mrad (±3°) up to almost 100 Hz and that it shows a continuously declining maximum scan amplitude for frequencies between 100 Hz and the system bandwidth of 1 kHz. At 1 kHz a small signal amplitude of 0.14 mrad is still feasible, which equals a maximum acceleration of about 5.5e3 rad/s^2. The peak power consumption of one system axis within the limits of the used amplifier and the admissible area of operation is 86 W.

Fig. 9b shows the measured rms drive current required for varying scan amplitudes of a sinusoidal reference signal with 1 Hz, applied to the closed-loop system. It can be seen that up to 2.5° the measured current increases linearly with the scan amplitude. Towards larger scan amplitudes the slope of the rms current becomes less steep, until it eventually changes to a negative slope between 2.7° and 3°. The current reduction at large amplitudes results from the over-proportionally increasing negative actuator stiffness that supports the acceleration of the mover in the outer areas. The controller needs to reduce its output in this range to avoid a snap-in of the mover, reducing the overall required rms current. Due to mounting tolerances there is an offset current to maintain the zero position of the mover.

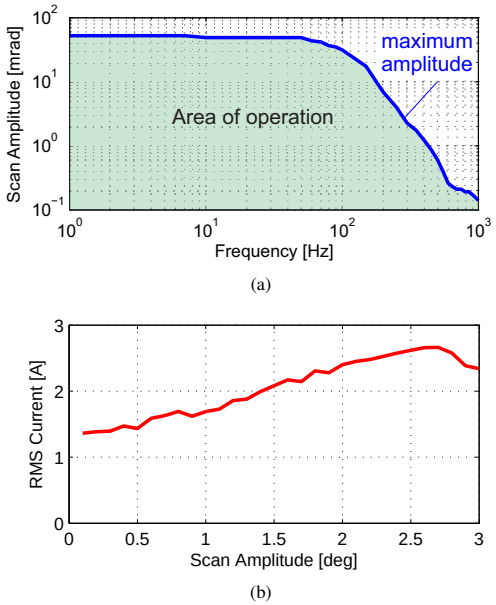

Fig. 9. Measured area of operation of the closed-loop hybrid actuator for sinusoidal reference signals. (a) shows the feasible scan amplitudes for frequencies within the closed loop system bandwidth. (b) depicts the required rms drive currents for various scan amplitudes of a 1 Hz sinusoidal reference.

For investigating the dual axis operation of the system various trajectories have been tested. Fig. 10a shows the fast system axis when tracking a raster trajectory with 30 Hz fast axis and 0.5 Hz slow axis frequency, and the maximum scan amplitude of 3°. Due to the current limitation higher fundamental frequencies of a triangular reference with maximum amplitude result in a distorted position signal. The peak-to-valley and rms tracking error is 0.262° (4.6 mrad) and 0.063° (1.1 mrad), respectively. Dual axis operation is demonstrated in Fig. 10b, which depicts the result of tracking a Lissajous trajectory [23] with frequencies of 40 Hz and 30 Hz for the x- and y-axis and an amplitude of 1.5°. The rms value of the areal tracking error, which is evaluated for each trajectory point, is

Post-print version of the article: E. Csencsics, J. Schlarp and G. Schitter, "High Performance Hybrid-Reluctance-Force-based Tip/tilt System: Design, Control and Evaluation," *IEEE Transactions on Mechatronics*, vol. 23, no. 5, pp. 2494-2502, 2018. DOI: 10.1109/TMECH.2018.2866272

0.012° (0.21 mrad). The angular resolution is evaluated at zero reference and results in a positioning uncertainty of 4.8 μrad rms.

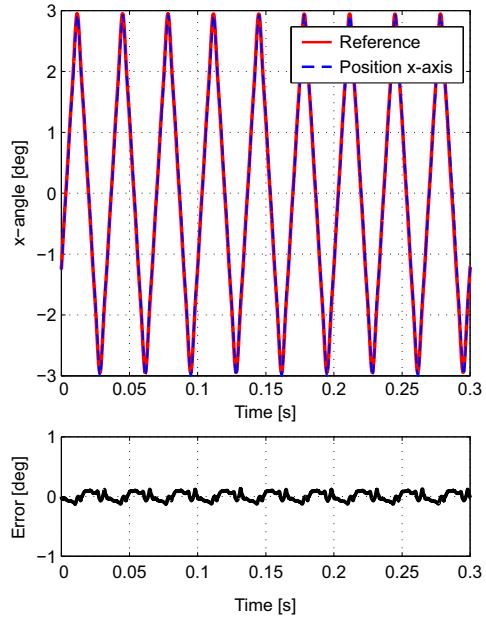

(a) Raster trajectory: fast axis motion and tracking error.

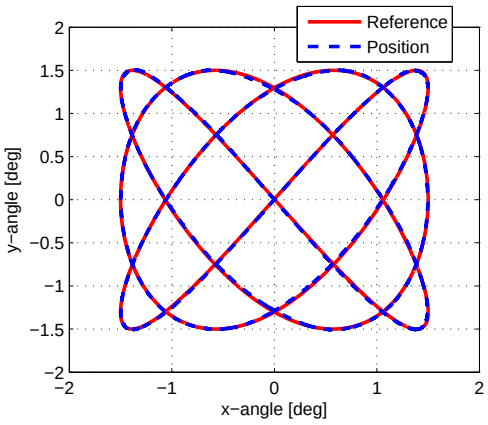

(b) Lissajous trajectory: dual axis motion.

Fig. 10. Measured trajectories. (a) shows the fast scan axis of the system tracking a raster trajectory with the maximum scan amplitude of 3°. The fast and slow scan axis have a fundamental frequency of 30 Hz and 0.5 Hz, respectively. (b) demonstrates dual axis operation, showing a tracked Lissajous trajectory with frequencies of 30 Hz and 40 Hz at a scan amplitude of 1.5°.

In summary the developed hybrid-reluctance-force actuator based 2DoF tip/tilt system prototype satisfies the targeted performance goals, providing large angular range and high system bandwidth at the same time.

VI. Conclusion

In this paper a novel 2DoF tip/tilt system design is proposed which is based on a new hybrid-reluctance actuator concept and may serve as basis for a new class of high performance tip/tilt positioning systems, such as e.g. fast steering mirrors. The actuator design relies on a symmetric hybrid reluctance force concept, that employs a single permanent magnet for biasing the integrated magnetic circuits of both actuation axes with a constant flux and two actuator coils per axis to generate a superimposed steering flux. The actuation concept allows an angular range of ±52 mrad (±3 deg) in tip and tilt and still enables a high closed-loop system bandwidth of 1 kHz. The angular range is significantly larger than in the case of the state-of-the-art reluctance actuated FSM with ±3.5 mrad [15] and piezo actuated FSM systems with e.g. ±2 mrad [3], and is comparable to the larger ranges that are achievable with voice coil actuated FSMs [4]. The product of range times bandwidth of the developed system results to 104 mrad·Hz, which clearly outperforms the state-of-the-art reluctance actuated FSM with 14 mrad·Hz (internal capacitive sensor, 2 kHz bandwidth) and 70 mrad·Hz (external optical sensor, 10 kHz bandwidth), respectively. Typical voice coil and piezo actuated systems with 61 mrad·Hz [2] and 12 mrad·Hz [3], respectively, are also clearly outperformed in this relation. Compared to the state-of-the-art reluctance actuated FSM with an angular resolution related to the entire angular range of 0.124e- 3, the angular resolution of the proposed system is with 0.046e-3 also improved. As the architecture allows to place the entire actuator behind the mover/mirror, the actuator appears suitable for miniaturization and may enable highly compact FSM as well as other mechatronic tip/tilt system designs.

Acknowledgment

The financial support by the Austrian Federal Ministry of Science, Research and Economy and the National Foundation for Research, Technology and Development, as well as MICRO-EPSILON MESSTECHNIK GmbH & Co. KG and ATENSOR Engineering and Technology Systems GmbH is gratefully acknowledged.

References

[1] M. Guelman, A. Kogan, A. Livne, M. Orenstein, and H. Michalik, "Acquisition and pointing control for inter-satellite laser communications," *IEEE Transactions on Aerospace and Electronic Systems*, vol. 40, no. 4, p. 1239, 2004.

[2] S. Xiang, P. Wang, S. Chen, X. Wu, D. Xiao, and X. Zheng, "The research of a novel single mirror 2d laser scanner," *Proc. of SPIE*, vol. 7382, Aug 2009.

[3] H. F. Mokbel, W. Yuan, L. Q. Ying, C. G. Hua, and A. A. Roshdy, "Research on the mechanical design of two-axis fast steering mirror for optical beam guidance," *Proceedings of 2012 International Conference on Mechanical Engineering and Material Science (MEMS 2012)*, 2012.

[4] M. Hafez, T. Sidler, R. Salathe, G. Jansen, and J. Compter, "Design and simulations and experimental and investigations of a compact single mirror tip/tilt laser scanner," *Mechatronics*, vol. 10, pp. 741–760, 2000.

[5] L. R. Hedding and R. A. Lewis, "Fast steering mirror design and performance for stabilization and single axis scanning," *SPIE Vol. 1304 Acquisition, Tracking and Pointing IV*, pp. 14–24, 1990.

[6] Q. Zhou, P. Ben-Tzvi, D. Fan, and A. A. Goldenberg, "Design of fast and steering mirror and systems for precision and laser beams and steering," *IEEE International Workshop on Robotic and Sensors Environments, Ottawa, CAN*, 2008.

[7] H. Yoo, M. E. van Royen, W. A. van Cappellen, A. B. Houtsmuller, M. Verhaegen, and G. Schitter, "Automated spherical aberration correction in scanning confocal microscopy," *Review of Scientific Instruments*, vol. 85, p. 123706, 2014.

Post-print version of the article: E. Csencsics, J. Schlarp and G. Schitter, "High Performance Hybrid-Reluctance-Force-based Tip/tilt System: Design, Control and Evaluation," *IEEE Transactions on Mechatronics*, vol. 23, no. 5, pp. 2494-2502, 2018. DOI: 10.1109/TMECH.2018.2866272

[8] F. M. Tapos, D. J. Edinger, T. R. Hilby, M. S. Ni, B. C. Holmes, and D. M. Stubbs, "High bandwidth fast steering mirror," *Optomechanics 200, Proceedings of SPIE Vol. 5877*, 2005.
[9] N. H. Vrijsen, J. W. Jansen, and E. A. Lomonova, "Comparison of linear voice coil and reluctance actuators for high-precision applications," *Power Electronics and Motion Control Conference (EPE/PEMC)*, 2010.
[10] A. van Lievenoogen, A. Toma, and U. Ummethala, "Challenges in the application of hybrid reluctance actuators in scanning positioning stages in vacuum with nanometer accuracy and mgauss magnetic stray field," *American Control Conference*, 2013.
[11] X. Lu, "Electromagnetically-driven ultra-fast tool servos for diamond turning," *Master's thesis, Massachusetts Institute of Technology*, 2005.
[12] D. Wu, X. Xie, and S. Zhou, "Design of a normal stress electromagnetic fast linear actuator," *IEEE Transactions on Magnetics*, vol. 46, no. 4, pp. 1007–1014, 2010.
[13] J. Kim and J. Chang, "A new electromagnetic linear actuator for quick latching," *IEEE Transactions on Magnetics*, vol. 43, no. 4, pp. 1849–1852, 2007.
[14] D. Laro, R. Boshuisen, J. Dams, and J. van Eijk, "Linear hybrid actuator for active force cancellation," *International Symposium on Linear Drives for Industry Applications*, vol. 8, 2011.
[15] D. J. Kluk, M. T. Boulet, and D. L. Trumper, "A high-bandwidth, high-precision, two-axis steering mirror with moving iron actuator," *Mechatronics*, vol. 22, no. 3, pp. 257–270, Apr 2012.
[16] M. Boulet, "Design of a small fast steering mirror for airborne and aerospace applications," *Master's Thesis, Massachusetts Institute of Technology*, 2008.
[17] Y. Long, C. Wang, X. Dai, X. Wei, and S. Wang, "Modeling and analysis of a novel two-axis rotary electromagnetic actuator for fast steering mirror," *Journal of Magnetics*, vol. 19, no. 2, pp. 130–139, 2014.
[18] R. M. Schmidt, G. Schitter, A. Rankers, and J. van Eijk, *The Design of High Performance Mechatronics*, 2nd ed. Delft University Press, 2014.
[19] E. Csencsics, J. Schlarp, and G. Schitter, "Bandwidth extension of hybrid reluctance force based tip/tilt system by reduction of eddy currents," *IEEE International Conference on Advanced Intelligent Mechatronics (AIM)*, 2017.
[20] S. Ito and G. Schitter, "Comparison and classification of high-precision actuators based on stiffness influencing vibration isolation," *IEEE Transactions on Mechatronics*, vol. 21, no. 2, p. 1169, 2016.
[21] E. Csencsics and G. Schitter, "Parametric pid controller tuning for a fast steering mirror," *IEEE Conference on Control Technology and Applications*, pp. 1673–1678, 2017.
[22] G. F. Franklin, D. J. Powell, and M. L. Workman, *Digital Control of Dynamic Systems*. Prentice Hall, 1997.
[23] E. Csencsics, R. Saathof, and G. Schitter, "Design of a dual-tone controller for lissajous-based scanning of fast steering mirrors," *American Control Conference, Boston, MA, USA*, 2016.

Ernst Csencsics is postdoctoral researcher at the Automation and Control Institute (ACIN) at Vienna University of Technology. He received a MSc. and PhD degree in Electrical Engineering from TU Wien, Austria in 2014 and 2017, respectively. His primary research interests are on high performance mechatronic systems design, control of opto-mechatronic systems, precision engineering, and in-line metrology systems.

Johannes Schlarp received an MSc. in Electrical Engineering from the Vienna University of Technology, Vienna, Austria in 2017 and is currently pursing a PhD degree with the Automation and Control Institute of the Vienna University of Technology, Vienna, Austria. His primary research interests are on high performance mechatronic systems and precision engineering for automated in-line metrology.

Georg Schitter is Professor at the Automation and Control Institute (ACIN) of the Vienna University of Technology. He received a MSc. in Electrical Engineering from TU Graz, Austria (2000) and his PhD degree from ETH Zurich, Switzerland (2004). His primary research interests are on high-performance mechatronic systems and multidisciplinary systems integration, particularly for precision engineering applications in the high-tech industry, scientific instrumentation, and mechatronic imaging systems, such as scanning probe microscopy, adaptive optics, and lithography systems for semiconductor industry.

Post-print version of the article: E. Csencsics, J. Schlarp and G. Schitter, "High Performance Hybrid-Reluctance-Force-based Tip/tilt System: Design, Control and Evaluation," *IEEE Transactions on Mechatronics*, vol. 23, no. 5, pp. 2494-2502, 2018. DOI: 10.1109/TMECH.2018.2866272